JGR Atmospheres

RESEARCH ARTICLE
10.1029/2020JD033081

Evaluating Stratospheric Tropical Width Using Tracer Concentrations

Kasturi S. Shah[1], Susan Solomon[1], David W. J. Thompson[2], and Douglas E. Kinnison[3]

[1]Department of Earth, Atmospheric and Planetary Sciences, Massachusetts Institute of Technology, Cambridge, MA, USA, [2]Department of Atmospheric Science, Colorado State University, Fort Collins, CO, USA, [3]Atmospheric Chemistry Observations and Modeling Laboratory, National Center for Atmospheric Research, Boulder, CO, USA

Key Points:
- Two new methods of using tracer concentrations as indicators of stratospheric tropical width are developed and compared
- These methods are advances over previous approaches as they provide consistent results throughout the year and the depth of the stratosphere
- Tracer-based widths correlate with the turnaround latitude, critical level, and tropopause height metrics, depending on altitude and method

Supporting Information:
- Supporting Information S1

Correspondence to:
K. S. Shah,
ks7@mit.edu

Citation:
Shah, K. S., Solomon, S., Thompson, D. W. J., & Kinnison, D. E. (2020). Evaluating stratospheric tropical width using tracer concentrations. *Journal of Geophysical Research: Atmospheres*, *125*, e2020JD033081. https://doi.org/10.1029/2020JD033081

Received 11 MAY 2020
Accepted 17 SEP 2020
Accepted article online 18 OCT 2020

Abstract Quantifying the width of the tropics has important implications for understanding climate variability and the atmospheric response to anthropogenic forcing. Considerable effort has been placed on quantifying the width of the tropics at tropospheric levels, but substantially less effort has been placed on quantifying the width at stratospheric levels. Here we probe tropical width in the stratosphere using chemical tracers, which are accessible by direct measurement. Two new tracer-based width metrics are developed, denoted here as the "1σ method" and the gradient weighted latitude (GWL) method. We evaluate widths from three tracers, CH_4, N_2O, and SF_6. We demonstrate that unlike previously proposed stratospheric width methods using tracers, these metrics perform consistently throughout the depth of the stratosphere, at all times of year and on coarse temporal data. The GWL tracer-based widths correlate well with the turnaround latitude and the critical level, where wave dissipation occurs, in the upper and midstratosphere during certain months of the year. In the lower stratosphere, the deseasonalized tracer-based widths near the tropical tropopause correlate with the deseasonalized tropopause-height based metrics. We also find that tracer-tracer width correlations are strongest at pressure levels where their chemical lifetimes are similar. These metrics represent another useful way to estimate stratospheric tropical width and explore any changes under anthropogenic forcing.

Plain Language Summary Studies of the expansion of the Earth's tropical belt have focused on the surface and the troposphere, with limited consideration to changes in the stratosphere. Further, these studies largely use measures of tropical width that depend on dynamical quantities like vertical and longitudinal velocities, stream function, and tropopause height. Changes to the position of the subtropical jet and to tropopause height have implications for stratospheric transport, mixing and upwelling strength as well as for long-lived trace gas variability in the lower stratosphere, motivating study of the width of the stratospheric tropics and potential metrics here. In this study, we argue that chemical tracers form a useful basis for stratospheric tropical width measurements, particularly for species that are directly measured. We develop two new tracer-based metrics that we call the 1σ method and the gradient weighted latitude method. These metrics advance opportunities to measure changes in stratospheric tropical width and to assess relationships between tropospheric and stratospheric width changes.

1. Introduction

Evidence for surface and tropospheric tropical expansion has been presented in several recent studies (Davis & Rosenlof, 2012; Grise et al., 2019; Lucas et al., 2014; Staten et al., 2018). Results vary depending upon the metric used (Davis & Rosenlof, 2012; Grise et al., 2019), heightening the need to develop consistent tropical width metrics and improve understanding of the drivers of changes to tropical width. Proposed influences on tropical width include stratospheric influences such as ozone depletion-induced cooling and volcanic aerosol-induced warming (Grise et al., 2019; Lucas et al., 2014; Staten et al., 2018). Additionally, shifts in the subtropical jet and changes to tropopause height influence stratospheric transport, mixing and upwelling strength, consequently influencing trace gas variability in the upper troposphere lower stratosphere. While measuring tropical width in the troposphere has been the focus of several recent studies, metrics of stratospheric tropical width have received considerably less attention.

A weakness of existing tropical width studies is that they generally use models which neither satisfactorily resolve stratospheric processes nor stratosphere-troposphere interactions (Seidel et al., 2008). Specifically,

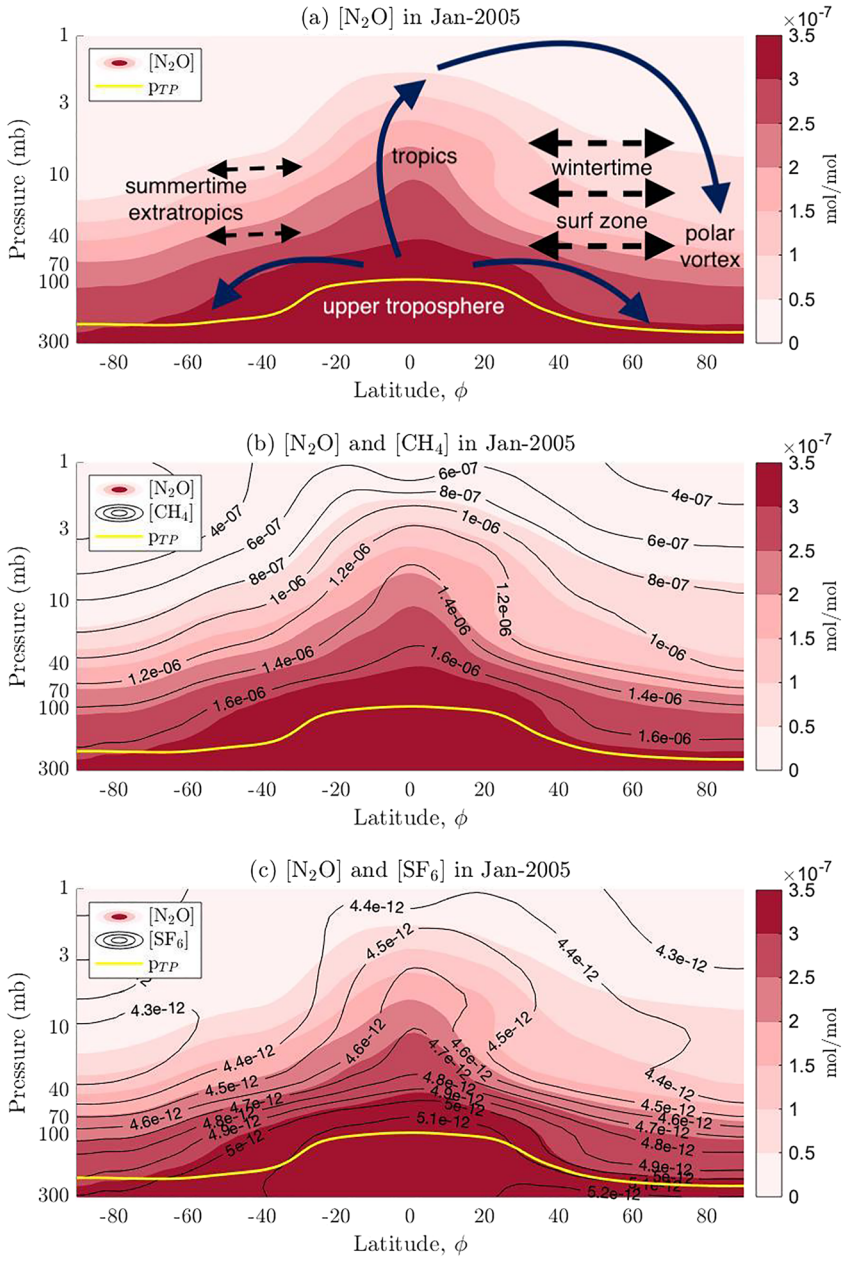

Figure 1. Ensemble mean, zonal mean tracer concentrations in January 2005: (a) N_2O annotated with dynamical regions in the stratosphere, (b) N_2O overlaid with CH_4 contours, and (c) N_2O overlaid with SF_6 contours.

low-top models have weak stratospheric variability on daily and interannual timescales, anomalously strong tropical upwelling strength, and a narrower tropical pipe than high-top models (Charlton-Perez et al., 2013). Furthermore, although tropical width studies exist that correlate width metrics using the zonal momentum balance against those using the vertical temperature structure (e.g., Solomon et al., 2016), they do not examine widths from stratospheric metrics that are applicable specifically above the tropopause. Tropospheric width metrics focus on the Hadley cell edge because of its relevance to surface climate, while stratospheric width depends on the position of tropical transport barriers and the edge of the upwelling zone, because of their relevance to stratospheric climate. Further, detecting tropical tropospheric expansion has focused on surface and tropospheric metrics largely obtained from derived dynamical quantities such as the stream function, vertical velocities, meridional velocities, and tropopause height

that are inferred from remote-sensing observations. Tracer-based metrics employ remote sensing observations directly but have been given less consideration. In this study, we develop robust stratospheric tracer-based metrics. We make use of simulations with the Whole Atmosphere Community Climate Model (WACCM) in a free running version with interactions between dynamics and chemistry.

Long-lived chemical tracers, such as N_2O and CH_4, are produced in the troposphere and destroyed in the stratosphere. These tracers, together with conserved tracers such as SF_6, exhibit maximum concentrations in upwelling regions in the tropics. This is because the primary entry point for tropospheric air into the stratosphere is through the tropical tropopause. Tracer concentrations vary relatively little with latitude within the stratospheric tropics (see Figure 1). Tracers experiencing stratospheric chemical loss display a latitudinal concentration gradient away from the tropics that depends upon the balance between upwelling, chemical loss processes, and quasi-horizontal mixing (Holton, 1986). Their concentrations decrease as air parcels experience chemical loss at higher altitudes and as air from higher altitudes moves laterally to higher latitudes, mixes, and descends. Steep concentration gradients are often found as air moves outside the tropics, as illustrated in Figure 1a for January 2005, as an example. Tracer concentrations can therefore be used to probe aspects of tropical width including the horizontal extent of the Brewer-Dobson circulation (BDC), changes in the strength of quasi-horizontal isentropic mixing and the injection of tropospheric air into the stratosphere at the tropical tropopause.

Tracers such as N_2O and CH_4 that experience chemical loss have contours that track each other closely over much of the stratosphere (Figure 1b). However, their equator-to-pole structures differ, for example, at 3mb and 70mb pressure levels, reflecting, we argue, the importance of differences in chemical lifetimes (Brasseur & Solomon, 2005). The influence of chemistry can be clearly discerned by comparing distributions of N_2O and SF_6 (Figure 1c). While distributions of N_2O and SF_6 are affected by vertical and horizontal advection and mixing, the distribution of N_2O is affected by stratospheric chemical loss as well, especially at higher altitudes. SF_6, in contrast, is essentially conserved throughout the stratosphere (although it does undergo some destruction in the mesosphere and thermosphere) and its surface mixing ratio linearly increases with time. N_2O and SF_6 contours track each other closely in the lower stratosphere. SF_6 contours maximize in the deep tropics, corresponding to the region of fastest upward residual vertical velocities (shaded red in Figure 2a). The wintertime surf zone, schematically marked in Figure 1a, corresponds broadly to the red regions of westerly zonal winds ($\overline{u} > 0$) depicted in Figure 2b and is marked by strong horizontal mixing and flattening of the tracer contours. The westerly zonal winds allow planetary wave propagation and wave breaking, which deposit easterly momentum and drive a stronger meridional circulation (as well as stronger local mixing). Both N_2O and SF_6 contours in the subtropics are steeper in the wintertime (northern) hemisphere than in the summertime (southern) hemisphere. Figure 2c overlays SF_6 and potential temperature contours and illustrates that the SF_6 contours slope increasingly more steeply with respect to potential temperature contours in the winter hemisphere than the summer hemisphere, reflecting faster downwelling.

We focus on the following key width metrics: (i) the latitude where concentrations deviate by more than 1σ from the average value found in tropical latitudes (1σ method) and (ii) the gradient-weighted latitude which measures the first moment of gradients in tracer concentrations between tropical and extratropical air (gradient weighted latitude [GWL] method), using the basic framework discussed in Davis and Rosenlof (2012) for a new application. We apply these metrics on both 3-D (longitude × latitude × pressure) and zonal mean (latitude × pressure) data.

Three other tracer-based stratospheric tropical width metrics have been examined in previous studies: the "PDF method," the latitude of steepest zonal mean tracer gradient, and total column ozone (TCO)-based metrics. The first two were developed to measure transitions between stratospheric dynamical regions. One metric uses the minimum in a tracer concentration's probability density function (PDF) at a given pressure level, where concentrations are a function of latitude and longitude, to identify a subtropical valley (Neu et al., 2003; Sparling, 2000). That is, the PDF for a tracer at a given pressure level is found by binning the data (over all latitude, longitude, and time) by concentration value. This metric works when a minimum in the tracer PDF exists. In practice, the minimum may be obscured by entrainment of air masses into and out of the subtropics. Stiller et al. (2017) use the PDF method on satellite data to explain the hemispheric asymmetries in stratospheric age of air trends. They detect a southward trend in the latitudinal position of the subtropical transport barriers in both hemispheres, correct the age of air distribution accordingly, and

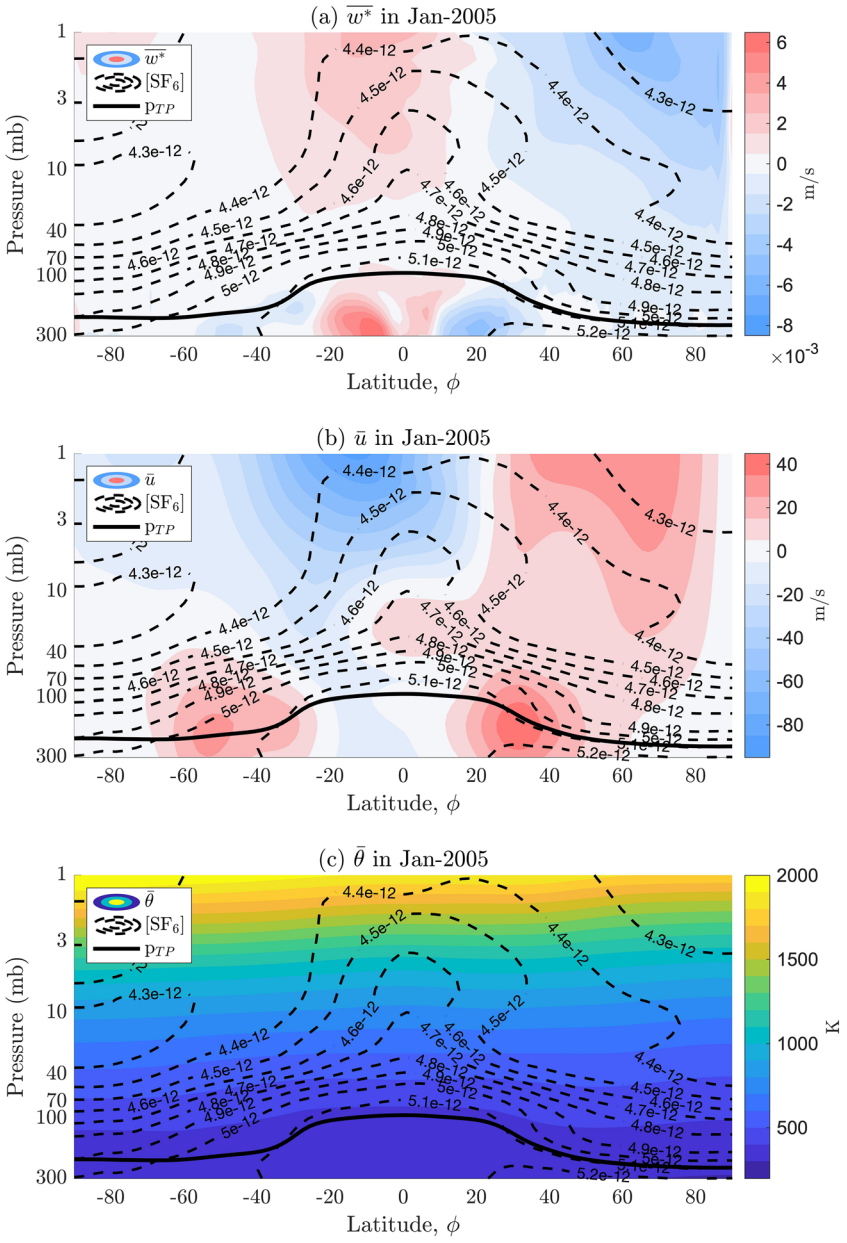

Figure 2. Ensemble mean, zonal mean SF_6 concentrations in January 2005 underlaid with color contours of the ensemble mean, zonal mean (a) Transformed Eulerian Mean residual vertical velocity, (b) zonal wind, and (c) potential temperature.

show that the southward trend is predominantly responsible for the hemispheric asymmetries because it shifts the entire stratospheric circulation southward. Another proposed metric in Sparling (2000) is the latitude of steepest zonal mean (and a variation they propose, the zonal mode) tracer gradient, which they criticized because the zonal average tracer gradient can be smeared across a broad latitudinal region by wave motions (Sparling, 2000). The tracer gradient method can be improved using 3-D rather than zonal mean values, but it can also be taken a step further by using a gradient weighted latitude approach, following Davis and Rosenlof (2012), to more robustly identify the steepest region. Here we show that calculating a gradient-weighted latitude (i.e., the first moment of tracer concentrations gradients) is a more robust metric than the steepest gradient metric and can be applied to both three-dimensional data and zonal averages.

A third stratospheric tropical width metric uses TCO values to identify changes in the subtropical and polar edges (Hudson et al., 2003). The changes in zonal TCO are not only due to changes in ozone abundances but also due to an increased relative area in the tropics and a decreased relative area near the poles, induced by the northward movement of subtropical and polar edges (Hudson et al., 2006). However, ozone is not strictly a tracer since it is affected by local production and loss chemistry as well as transport. It is also influenced by human-induced ozone depletion. Hence, its use as a tracer for changes in width is compromised by such factors as ozone depletion trends (Lamarque & Solomon, 2010) and by perturbations to chemistry, such as temporal changes in water vapor. In-depth analysis has indicated the sensitivity of TCO to the width-measuring algorithm, data inconsistencies in the northern hemisphere, and lack of correlation with other metrics on interannual timescales (Davis et al., 2018), making it difficult to use to assess tropical width. In summary, existing stratospheric tracer-based metrics cannot be applied at all stratospheric pressure levels nor on coarse temporal resolution data nor over all seasons, limiting their utility. These studies provided a useful basis for considering dynamical transitions in tracer behavior between the tropics and extratropics at the time they were introduced; here we build upon these findings with the availability of new models and data.

We have laid out this paper as follows: We describe the model output and the metrics we use in more detail in section 2. We test the metrics' sensitivity and robustness by analyzing how different tracer metrics compare with each other and across different tracers in section 3. We explore the physical processes measured by tracer-based metrics of tropical width in section 4. We discuss applications to which tracer-based metrics are particularly suited, as well as instances in which tracer-based metrics fail, and summarize our conclusions in section 5.

2. Data Sets and Methods

2.1. Model Output

We describe here the model and the simulations that we use in this study. We analyze free-running (FR) simulations of the Whole Atmosphere Community Climate Model (CESM1 WACCM4) with a fully interactive atmosphere and ocean in a perturbed state near the period of maximum ozone losses, with fully interactive chemistry. The run we analyze covers the period of ozone depletion 1995–2024 with greenhouse gases (GHGs) and ozone depleting substances (ODSs) following RCP6.0. The run has 10 ensemble members with monthly output. Below, we discuss tropical widths that we measure from the ensemble mean of monthly ensemble output along with the standard deviation in tropical widths that we measure from each of these 10 ensemble members individually to indicate the influence of variability due to dynamical changes, which is one measure of the spread in ensemble results. Further details about the model can be found in the supporting information (Text S6.2). We outline the data used in this study in Table S1.

N_2O, SF_6, and CH_4 are subject to trends in their tropospheric abundances due to increasing emissions. Removal of such trends is required if changes in the width of the tropics are to be accurately identified using these tracers. Section 6.3 and Figures S1 and S2 in the supporting information detail how anthropogenic trends are removed. The anthropogenic trend has been removed prior to conducting all analyses in this study.

2.2. Tropical Width Metrics Used in This Study

The tropical width metrics explored in this study are presented in Table 1 and depicted in Figure 2. We next discuss these metrics and relationships between them. We examine three-tracer based metrics in this study: the 1σ method (which we propose, Figure 3a), the GWL (Figure 3b) metric (which we propose, following Davis and Rosenlof, 2012, who apply this method to tropopause height) and the PDF method (Neu et al., 2003; Sparling, 2000). We also examine two dynamical metrics for stratospheric tropical width, the turnaround latitude (where $w^* = 0$) and the critical level where stationary Rossby waves break (at $\overline{u} = 0$), and three tropopause height-based metrics (Table 1). The tracer-based metrics measured at 5mb and the tropopause height-based metrics are plotted in Figure 3c with the standard deviation in widths from the 10 ensemble members.

Latitudinal tracer concentration distributions at each pressure level are largest in the tropics. These distributions vary less with latitude there compared to midlatitude or polar regions (see Figure 1). What will be referred to here as the 1σ method is a way to measure the horizontal extent of the region of tropical tracer

Table 1
Tropical Width Metrics Explored in This Study

Metric	Class	Definition	Temporal resolution	References
1σ	Tracer	Latitude at which tracer concentrations deviate by 1σ from its tropical mean.	D&M	This study
GWL	Tracer	Latitude weighted by the gradient in tracer concentrations	D&M	This study, after Davis and Rosenlof (2012) approach for z_{TP}
PDF	Tracer	Latitude of subtropical minimum in the probability density function (PDF) of tracer concentrations	D	Sparling (2000) and Neu et al. (2003)
$\overline{w^*} = 0$	Velocity	Latitude at which the Transformed Eulerian Mean residual vertical velocity equals zero	D&M	Neu et al. (2003)
$\overline{u} = 0$	Velocity	Latitude at which the zonal mean zonal wind equals zero	D&M	Neu et al. (2003)
$z_{TP} = 15$ km	Tropopause height	Critical threshold for z_{TP}	M	Davis and Rosenlof (2012)
$\Delta z_{TP} = 1.5$ km		Latitude of tropopause break	M	
GWL z_{TP}		Gradient-weighted latitude in z_{TP}	M	

Note. D = daily, M = monthly.

concentrations. The 1σ method marks the latitude where the meridional gradient of concentrations at a given longitude, pressure level, and time step deviates by one (spatial) standard deviation (1σ) from the spatial mean, where the spatial standard deviation and mean are calculated over the 70° latitudinal range containing the highest tracer concentration values. In section 3.1, we show how this method would be affected if values narrower or broader than 70° are chosen. While the 70° latitudinal range often corresponds to 35N–35S, the method accounts for any "leaning" of the tropics into one or the other hemisphere. The 1σ method thus measures the latitude at which the tracer concentrations fall away from the tropical maximum values. For example, consider the meridional profile of tracer $\chi(\phi)$ at a given longitude, pressure level, and time step, where ϕ represents latitude. If the 70° latitudinal range containing the highest concentrations of $\chi(\phi)$ corresponds to ϕ_N°N and ϕ_S°S, then the edge of the tropics is defined as the latitude where $\chi <$ [mean(χ) − std(χ)], where the mean and standard deviation are calculated from values of $\chi(\phi)$ between ϕ_N°N and ϕ_S°S. An illustration of the 1σ method applied at 120°E, at 5mb, in January 2005 to N_2O concentrations in the Northern Hemisphere (NH) is shown in Figure 3a. In this case, the 70° latitudinal range containing the highest concentrations is 25°S to 44°N, and the mean and standard deviation of the concentrations in this range are 1.16×10^{-7} and 3.67×10^{-8}mol/mol, respectively. The NH latitude at which the concentration crosses the 1σ threshold (that is, 1.16×10^{-7} to 3.67×10^{-8}) is 31.3°N in this example (Figure 3a).

The tropical pipe model for stratospheric transport (Plumb, 1996) assumes a dynamically isolated tropical region, in which horizontal mixing into the tropics is negligible compared to the net vertical (upward) motion. It envisions a pipe through which stratospheric transport occurs from the tropopause to the upper stratosphere. While other definitions could be used, the 1σ method is based on this conceptual model and is one way to identify a latitude of the pipe's edges.

The GWL metric is also illustrated in Figure 3b and indicates the balance between the diabatic circulation (steepens gradient), quasi-horizontal mixing by large-scale eddies (flattens gradient), and chemical loss for active species (steepens gradient if loss occurs in the extratropics) (Holton, 1986). Stratospheric chemical loss can create a gradient as air is advected into regions where chemical destruction is faster than resupply via transport or where a switch from upward to downward motion brings tracer-depleted air down from above more quickly than transport can replace it. Sparling (2000) briefly mentions the latitude of steepest tracer gradient as a potential metric but uses zonal mean data to calculate it and concludes that the latitudinal region is too broad to identify an edge. The steepest tracer gradient method is sensitive to intrusions of filaments or wave motions that bring tracers into and out of the tropics (and the same applies to the 1σ or PDF methods), such as those shown in Figure S3. This means that the steepest gradient method is sensitive to the horizontal resolution of the data. Here we calculate the GWL, which defines the region of steep gradients on both 3-D data and zonally averaged data. The GWL is calculated between the Equator and the pole in each hemisphere. We compute it in radians at each longitude, as follows

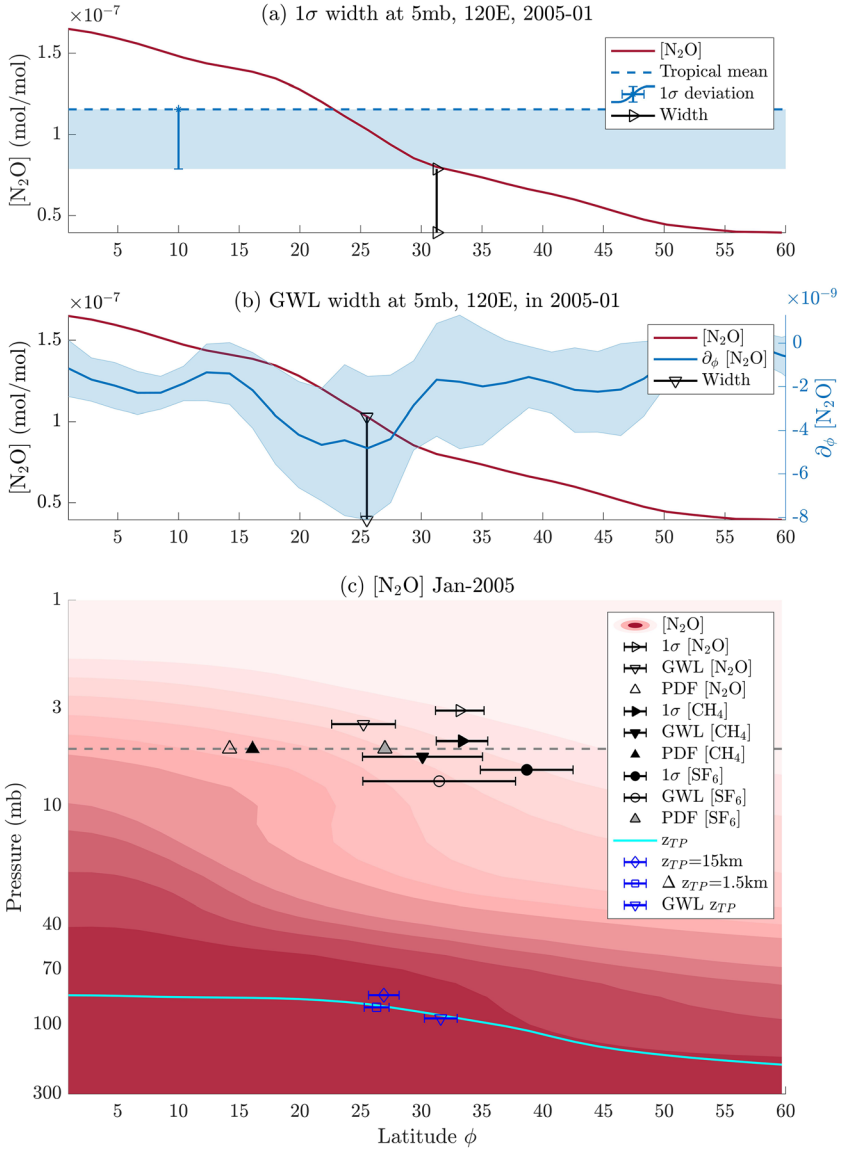

Figure 3. (a) Illustration of the 1σ method: in red is the N_2O concentration profile at 5mb, 120°E in January 2005, the blue-dashed line is the mean over the 70° latitudinal range of maximum N_2O values in both hemispheres, the blue shaded error bar indicates the threshold value of 1σ deviation from this mean. The black vertical line is the latitude with the closest concentration to that threshold value. (b) Illustration of the gradient-weighted latitude method: in blue is the tracer gradient as a function of latitude at 5mb, 120°E in January 2005. The blue shaded region represents the standard deviation in tracer gradient measured from individual ensemble members. The black vertical line marks the tracer gradient weighted latitude. (c) N_2O zonal mean ensemble mean concentrations in January 2005 contoured at intervals of 1.25×10^{-7} mol/mol. Ensemble mean tracer widths for N_2O, CH_4, and SF_6 at 5mb are marked with error bars to indicate the standard deviation in widths measured from the 10 ensemble members. The tracer widths have been offset from 5mb in the plot for clarity. Overlaid in cyan is the tropopause height, with three ensemble mean tropopause height metrics and their ensemble spread marked in blue. The z_{TP} = 15 km metric has been offset from the tropopause pressure for clarity.

$$\phi_i = \frac{\sum_{j=Eq}^{j=Pole} \phi_j \left(\partial_\phi \chi\right)_{ij} \cos\phi_j}{\sum_{j=Eq}^{j=Pole} \left(\partial_\phi \chi\right)_{ij} \cos\phi_j}$$

where *i* indexes over longitudes and *j* indexes over latitudes. Figure 3b illustrates the GWL metric applied at 120°E, at 5mb, in January 2005 to N_2O concentrations in the Northern Hemisphere. In this example, the GWL width is 25.5°N.

For both the 1σ method and GWL method, after evaluating the tropical boundary latitude at each longitude (for a given pressure level and day [or month]), we compute an area-equivalent width following (Davis & Rosenlof, 2012)

$$\phi_{eq} = \sin^{-1}\left(\frac{\sum_{i=1}^{n}\sin\phi_i}{n}\right)$$

where n is the number of longitude levels (in our model output $n = 144$; see Table S1). This area equivalent width (ϕ_{eq}) is computed for ϕ_i measured from both the 1σ and GWL methods at every pressure level and shown in Figure 3c. ϕ_{eq} is the tropical width measured from 3-D (latitude × longitude × pressure) data, and this area-equivalent latitude is presented in all the figures below. Both 1σ and GWL metrics have also been run on longitudinally averaged data, where the zonal mean latitudinal distribution at each pressure level is evaluated to measure tropical width. Widths measured from 3-D and zonal mean data are compared in section 3.5.

The third tracer-based metric we examine is the previously published PDF method for determining the subtropical edge. The subtropical edge can be located by a minimum in the PDF of tracer concentrations at each pressure level (Neu et al., 2003; Sparling, 2000). We describe and illustrate this method in the supporting information (Text S6.4 and in Figures S3–S5) and find that the minimum in the PDF is more easily distinguishable for months that fall clearly into a summer/winter dynamical pattern (August and Sept in Figure S3) than for months that do not (October in Figure S5). We assess the sensitivity and robustness of the tracer-based metrics in section 3.

Two velocity-dependent dynamical metrics and three tropopause height-based metrics are also compared against tracer-based width metrics here. The $w^* = 0$ metric measures the turnaround latitude between ascending/descending branches of the BDC. The $\overline{u} = 0$ line marks the critical level at which non-linear dissipative effects such as horizontal mixing can begin (Leovy, 1987). As Figure 1a depicts, increased horizontal mixing is a characteristic of high latitudes. Transport out of the tropics in the winter hemisphere is related to the appearance of westerlies at the start of the season, which causes initial wave-breaking, followed by vertical-wave propagation through the tropics (without wave breaking). When the summer easterlies begin, the subtropical edge shifts quickly equatorward (Neu et al., 2003). Each velocity metric measures different but related dynamical processes of the tropics and extratropics (Neu et al., 2003), and we compare the tracer-based and dynamical metrics in section 4. We also discuss how tracer-based width measurements compare to the three tropopause height-based width measurements listed in Table 1.

3. Sensitivity and Robustness of Tracer-Based Width Metrics

In this section, we discuss sensitivities of the tracer methods to different factors, compare them to one another, and analyze how readily they can be applied for different altitude ranges.

3.1. Robustness of Gradient Weighted Latitude Versus Steepest Gradient Method

We measure the GWL and steepest gradient widths over the 30-year period 1995–2024 in 10 ensemble members. We assess the robustness of the GWL method versus a simpler 3-D steepest gradient method by determining which method has a narrower variance in ensemble widths. A time series of widths is plotted at 5mb and 73mb in Figures S7a, S7b, S7d, and S7e. We note that the GWL metric and the steepest gradient metric are positively correlated (with coefficients of ~0.76 at 5mb and 0.62 at 73mb) and significant at the 95% level.

The ratio of the ensemble variance at 5mb and 73mb is plotted as a function of time in Figures S7c and S7f. We plot the ratio of the ensemble variance computed on temporal mean widths at each pressure level in Figure S7h. We conduct *f* tests at each pressure level and find that below 2mb, the variance in steepest gradient widths is generally larger than the variance in GWL widths, indicating that the GWL widths have a narrower spread from each ensemble member than the steepest gradient widths. We therefore conclude that the GWL method is generally more robust than the steepest gradient method over most of the stratosphere. Throughout the rest of this study, we consider pressure levels below 2mb.

In addition to having a tighter ensemble spread than the steepest gradient method, the GWL method detects the shift in the center of mass of a distribution over a range of latitudes and is not sensitive to

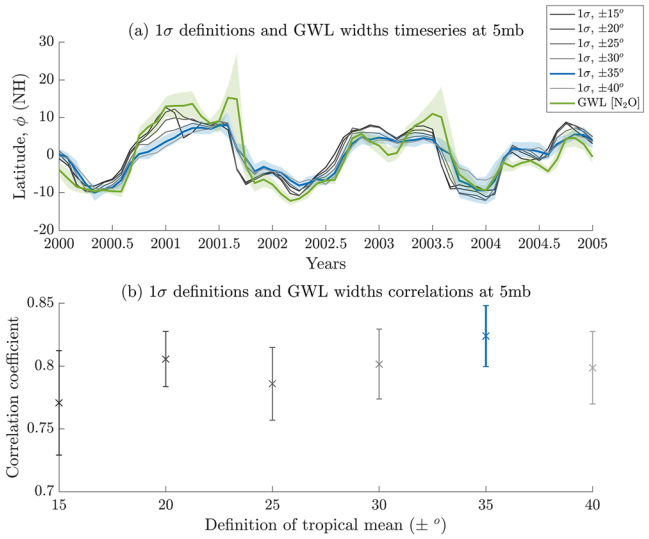

Figure 4. (a) Sensitivity of ensemble mean 1σ method to the range over which the tropical mean is defined. All the widths plotted here (and in the rest of this paper) are the area-equivalent latitude computed from widths measured at each longitude. Here the definition of the tropical mean is varied over a range of ±15° to ±40°, in 5° increments. These definitions are compared to widths measured by the GWL method at 5mb (in green, with a shaded error bar representing the standard deviation of widths from ensemble members). The ±35° definition of tropical mean is plotted in blue with a shaded error bar representing the standard deviation of widths from ensemble members. (b) Correlation coefficients between the 1σ widths measured for each definition of tropical mean and the GWL widths over the entire 30-year period (1995–2024) are plotted with error bars representing the one standard deviation in correlations across ensemble members.

noise (Davis & Rosenlof, 2012). It is also not limited by the model resolution even when measuring width on zonally averaged data, and it therefore represents a useful improvement over the steepest gradient method.

3.2. Sensitivity of 1σ Method to the Latitude Range Over Which to Define a Tropical Mean

In order to assess the sensitivity of the 1σ method to the latitude range of the tropical mean, we vary this range from ±15° to ±40° in 5° increments. The widths measured by each definition of tropical mean are plotted in Figure 4a for the years 2000–2005 at 5mb, as an example chosen for consistency with Figure 3, and compared to widths measured by the gradient weighted latitude (thick green line). The sensitivity that the 1σ method exhibits at 5mb is consistent with its sensitivity at other stratospheric pressure levels. We provide the full 30-year time series for these 1σ width definitions and the GWL widths at 5mb over the entire temporal period of the model output (1995–2024) in Figure S8. Defining the 1σ widths based on a narrow latitudinal window pushes the tropical widths markedly equatorward during the start of the winter in the Northern Hemisphere. These months are when the westerly zonal winds and the turnaround latitude intrude into the tropics, perturbing tracer contours (section 4). Figure 4a suggests that the ±35° definition (thick blue line) agrees fairly consistently with the GWL widths. We note that the GWL widths do not perfectly align with the 1σ widths measured from any chosen tropical interval. For instance, at the start of the time series it matches up with the ±15° definition of the 1σ method, while at the end of the time series it matches up with the ±35° definition. The coincidence of these two metrics does not mean that they are measuring the same aspect of tropical width.

Figure 4b shows correlations between 1σ widths (derived from each tropical mean definition in Figure 4a) and the GWL method. The ±35° definition of tropical mean (in blue) has the highest correlation coefficient and has one of the narrowest standard deviation in correlations among ensemble members. This analysis has been conducted at every pressure level (not shown), and on average, the ±35° definition for the tropical mean has the strongest correlation with the GWL widths. Therefore, for the rest of this study, the tropical mean is defined as the ±35° latitudinal window over which the 1σ method is applied.

3.3. Temporal Resolution at Which Metrics Can Be Applied

Figure S9 probes the question of the temporal resolution of data needed for tracer metrics. Two resolutions are examined, both using 3-D data: (i) temporal mean over all latitudinal widths measured from 3-D daily output and (ii) widths measured from monthly averaged values. The daily output in these figures was obtained by branching off the first ensemble member of the free-running WACCM run. This daily output run is another ensemble member of the free-running WACCM run. Resolutions (i) and (ii) agree well with each other for the 1σ and GWL methods in sample months shown (Figure S9). This indicates that these methods can be applied on tracer concentration data with coarser temporal resolution to reasonable accuracy. Therefore, widths can be measured from monthly output of WACCM simulations.

The PDF method's widths from daily and monthly output agree better with each other in certain months than in others. We emphasize that Neu et al. (2003) noted that their method works better for months that can be firmly categorized as summer or winter months. For illustration, here we show January and October. Consistent with Neu et al. (2003), we find better agreement in January than in October as measured by differences in widths (not shown) measured from daily and monthly output. However, the minimum in the monthly tracer PDF is not visible at certain pressure levels in either month. It is to be expected that the PDF method works much better on higher temporal resolution information, because each day of data provides more points with which to generate a more accurate PDF and a clearly identifiable subtropical edge. The minimum in the PDF is less visible for tracer concentration time series with longer temporal intervals

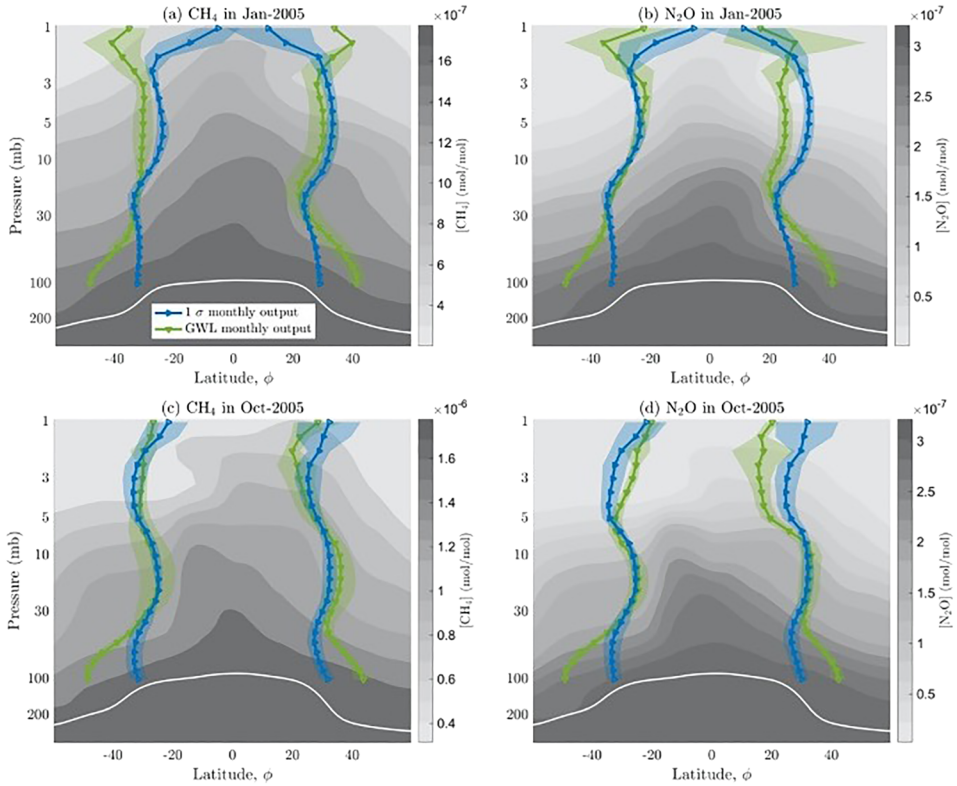

Figure 5. Comparing tracer-dependent metrics against each other and between the two tracers CH_4 and N_2O for (a and b) January and (c and d) October 2005. Ensemble mean tropical widths measured by the 1σ (blue) and GWL (green) methods for (a) CH_4 and (b) N_2O are shown with the standard deviation in ensemble members indicated by the shaded error bars. Only widths measured above the tropical tropopause (white line) have been shown.

between each datapoint, as the PDF is sparser and wave-driven excursions of air from tropical to subtropical latitudes (and vice versa) smear the contrasts between them in the monthly PDF. This makes identification of the subtropical valley more difficult and indicates that the PDF method is not appropriate for the underlying physics (Neu et al., 2003). Therefore, all PDF results presented in this study have been doubly verified for accuracy by also identifying the minimum by visual inspection. One aim of our study is to develop and improve methods that can be applied at all times of year and over the depth of the stratosphere.

We find that the 1σ and GWL metrics can be accurately applied at all times of year because they measure characteristics of tracer contours that are present regardless of the season. The PDF method breaks down in months when there is not a clear summer/winter pattern in the PDF from which to identify a minimum: see July/August/September 1992 (Figures S3 and S4) versus October 1991 (Figure S5), both from CLAES data.

Due to the agreement between widths measured from daily data and widths measured from monthly averaged data, for the rest of this study, monthly averaged output will be analyzed.

3.4. Comparing 1σ, GWL, and PDF Methods' Widths

We next illustrate how metrics compare during a month that falls clearly into the summer/winter seasons (January; Figures 5a and 5b) and during a month when seasonal dynamical patterns are transitioning in each hemisphere (October; Figures 5c and 5d). We illustrate this for CH_4 and N_2O as they, unlike SF_6, experience chemical loss. The ensemble mean widths are plotted and the spread in ensemble members is indicated by the shaded error bars in Figure 5. We also correlate the widths obtained for different species and methods at different pressure levels in section 4.3.

In January and October in the middle stratosphere, the 1σ and GWL methods are broadly consistent with each other, as is evident from each panel in Figure 5. In the lower stratosphere, the GWL widths are

generally poleward of the 1σ widths. In October, when mixing is weaker, widths from both methods are consistent with each other through the upper stratosphere (Figures 5c and 5d). Additionally, both GWL and 1σ width measurements capture the "lean" of tracer contours into the Southern Hemisphere during October. Horizontal mixing flattens the gradient in the subtropics and steepens the gradients at the tropical edge of the surf zone. In months such as January when (horizontal) mixing from wave breaking is strong, the GWL and the 1σ widths are pushed equatorward. This effect of wave motions on tracer contours is illustrated in Figure S6. Reasons for different behaviors between different metrics will be discussed further in section 4.2.

The PDF method's results fall within the range of widths measured by the 1σ and GWL methods at most pressure levels in January and some pressure levels in October (Figure S9). Particularly in October, however, they do not vary smoothly from one pressure level to the next. Generating the PDF involves horizontal integrations through the concentration-latitude scatterplot and, due to wave-induced entrainment of air masses, the PDF can sometimes form just one peak as the concentration gradient flattens (Figure S5). Therefore, not only is a clear minimum not visible in such cases but neither are dynamical features like the wintertime surf zone.

3.5. Vertical Depth Over Which Metrics Can Be Applied

Figure 5 shows that the 1σ and GWL methods can be applied throughout the stratosphere (1–100mb). In contrast, we find that the January minimum in tracer PDF is clearly identifiable only within the 1–30mb range (Figure S9), as also emphasized in Neu et al. (2003). This is because the strong mixing in the surf zone steepens tracer gradients at the subtropical edge of the surf zone. This forms a barrier to horizontal transport, leading to the formation of a minimum in the PDF at the latitude of this subtropical edge. The October minimum is obscured at some pressure levels due to the surf zone breaking up (southern hemisphere) and the surf zone forming (northern hemisphere); see Figure S5. The minimum gets harder to identify for higher pressures beyond this range due to wave-induced entrainment of air into the subtropics, which is particularly prevalent in the lower to middle stratosphere.

3.6. Comparing Results From 3-D (Lon × Lat × Pressure) Versus 2-D (Lat × Pressure) Data

Assessing stratospheric width changes would require multiple years of data, which may be more readily available for sparse data in a 2-D rather than 3-D observational grid. To determine the extent to which our metrics can be applied to 2-D (latitude × pressure) output, we next evaluate how the metrics perform on longitudinally averaged data (henceforth, called 2-D data). The absolute differences between ensemble mean widths measured from 3-D and 2-D data for monthly output are calculated for model years 1995–2024 and the temporal mean of these differences is plotted in Figures 6a–6c for the southern hemisphere. As noted in section 2, the PDF method requires 3-D daily data to produce the best-defined minimum in the PDF, such that there is limited smearing of values by wave motions, and such that there are a statistically significant number of points in each bin. Therefore, the PDF method has not been included in Figure 6.

The differences between 2-D and 3-D widths from the GWL method have a smaller magnitude than the differences from the 1σ widths, across both tracers and both hemispheres (only Southern Hemisphere shown in Figures 6a–6c). The differences measured from each metric are of comparable magnitude throughout the stratosphere, indicating that dynamical variability affects the tracer-based widths at all pressure levels. The differences and the ensemble standard deviation of the differences are larger for the 1σ method than for the GWL method, suggesting that the 1σ method has a wider spread in widths than the GWL method. Therefore, 3-D effects increase the variability of widths measured by the 1σ method more than for the GWL method. However, we note that the differences generally fall within a narrow range of $\pm 0.6^{o}$, indicating that both the 1σ and GWL method can be applied to 3-D and 2-D data with reasonable accuracy.

Widths from 3-D and 2-D data for the same tracer are correlated from 1995 to 2024 in Figure 6d. Correlations between the 3-D and 2-D widths measured from both the 1σ and GWL methods are very high (generally ≥ 0.90) and significant throughout the depth of the stratosphere in both hemispheres for all three tracers (CH_4, N_2O, and SF_6).

We conclude that 3-D dynamical effects such as horizontal mixing result in a wider ensemble standard deviation in 1σ widths than in GWL widths and that 1σ and GWL widths can be measured from both 3-D and 2-D data to reasonable accuracy.

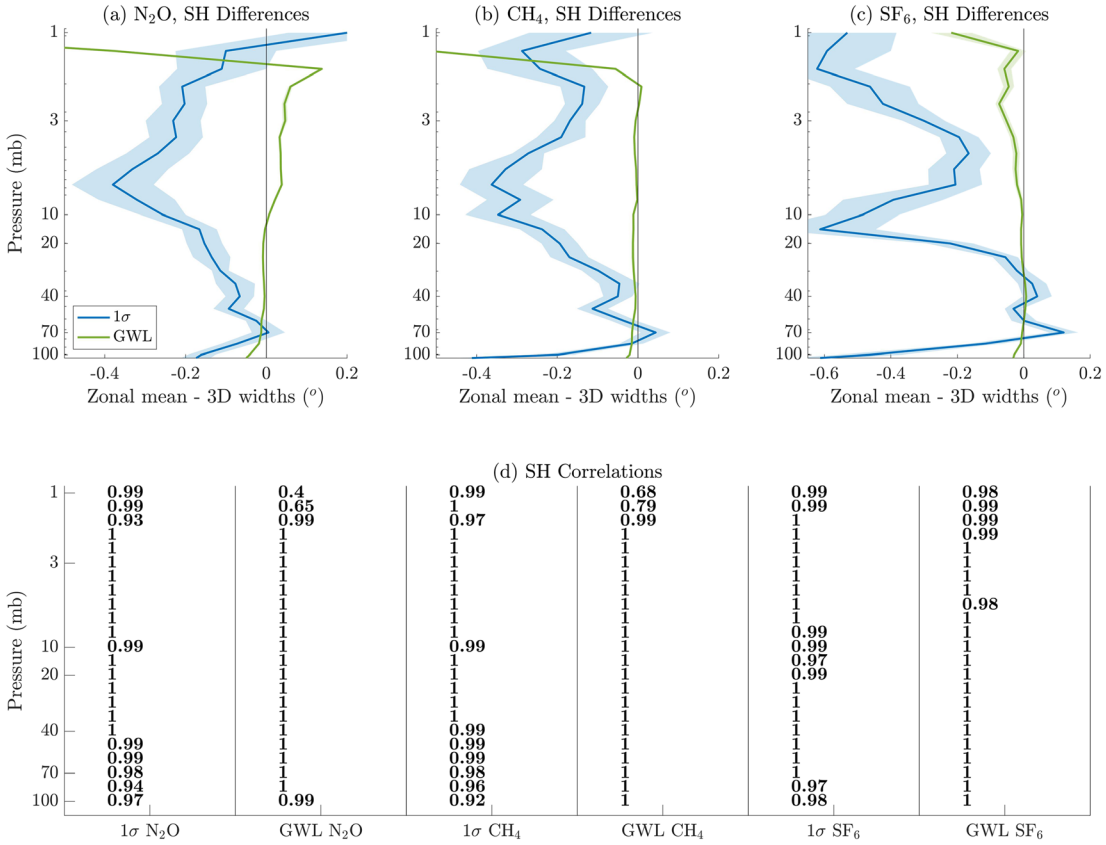

Figure 6. (a–c) Temporal mean ensemble mean differences 1995–2024 between ensemble mean widths measured from zonal mean versus 3-D data in the Southern Hemisphere. The standard deviation of temporal-mean differences measured from each individual ensemble member is marked with a shaded error bar. (d) Correlations 1995–2024 between these annual mean, ensemble mean widths from zonal mean and 3-D data at each stratospheric vertical level. Correlations that are significant at the 95% level are bolded.

4. Physical Processes Related to Tracer Metrics

The tracer fields over a longitude-latitude plane at each vertical level can exhibit a delayed response to dynamical changes, such as upwelling or horizontal mixing. For example, changes in vertical velocity need not result in immediate tracer concentration changes, because of the time required for transport. The delay timescale is influenced by the advective timescale, over which changes in the velocity field are able to influence tracer contours (e.g., by bringing down air depleted in N_2O or CH_4 from above, where chemical lifetimes are shorter). A vertical transport timescale for each tracer, τ_χ, can be calculated at each latitude as follows,

$$\tau_\chi = \frac{z_s}{w^*}$$

where w^* is the residual vertical velocity. z_s is the height over which the zonal mean concentration profile of tracer χ reduces by a factor of $\frac{1}{e}$ and is influenced by chemical loss as well as by transport. The tracer fields and tracer-based widths analyzed below have all been lagged using this transport delay timescale since this is required for the purposes of comparison to dynamical widths $w^* = 0$ and $\overline{u} = 0$. All correlations are conducted from widths over the 30-year period 1995–2024. (Analysis presented in previous sections has not been lagged with this timescale as no comparisons to velocity fields were made.)

4.1. Tracer Widths' Seasonal Cycles

We first examine the seasonal cycle in lagged tracer widths by overlaying them on the lagged tracer concentrations for N_2O and SF_6 at 5mb (Figures 7a and 7b) and at 13 mb (Figures 7c and 7d) and for CH_4 at the

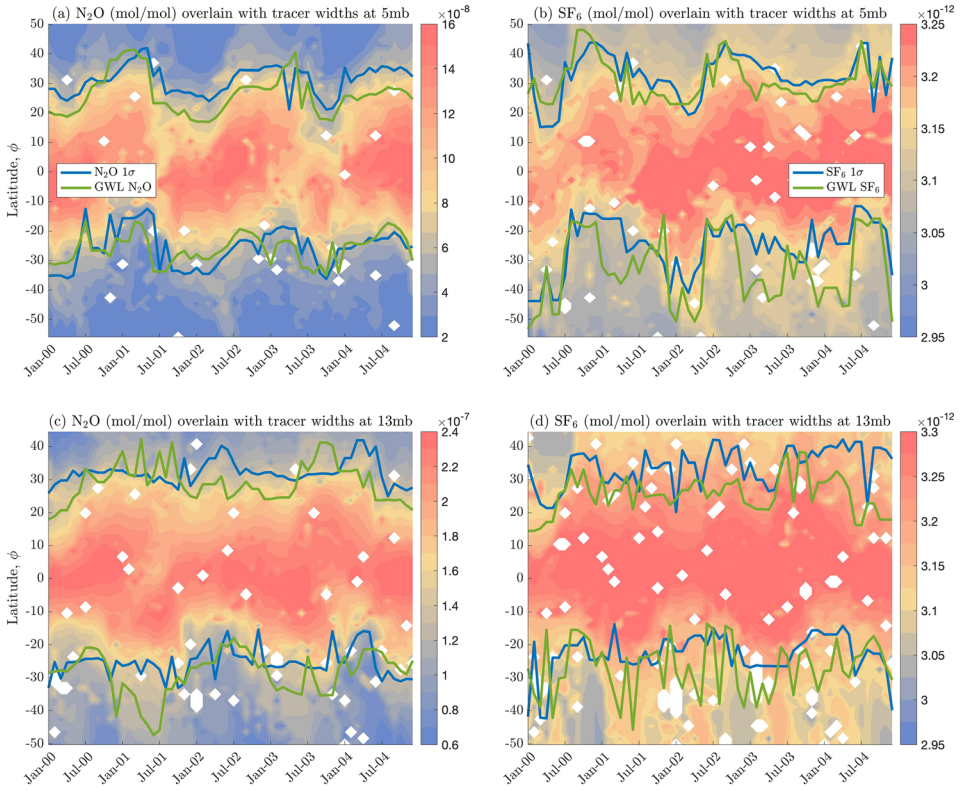

Figure 7. Underlaying ensemble mean tracer widths with their respective ensemble mean tracer fields at (first row) 5mb, (second row) 13mb for (left column) N_2O and (right column) SF_6. The 1σ widths are plotted in blue, and the GWL widths are plotted in green. Both the tracer fields and the tracer-based widths have been lagged by τ_χ. The white regions mark latitudes where anomalously long τ_χ occur due to anomalously small vertical velocities or anomalously large *e*-folding heights.

same pressure levels in Figure S10. The anthropogenic increases in each tracer have been removed (Text S6.3 in the supporting information). In Figure 7, the white regions mark latitudes where anomalously long lag timescales occur, due to anomalously small vertical velocities or anomalously large *e*-folding heights.

Both tracer fields and tracer-based widths have been lagged to illustrate the influence of dynamical motions on tracer fields over the five-year period 2000–2004. The lagged timescales are on average 4–5 months for N_2O and 6–7 months for SF_6. The motion of the widths corresponds to the movement of the regions of steep gradients and to how sharply the tracer concentrations fall away from their low latitude peak. The latter influences widths from the 1σ method.

Each tracer-based width exhibits a seasonal cycle. The tropical boundaries move equatorward during the winter months. The tracer contours steepen in the winter hemisphere due to mixing in the surf zone which pushes the region of steep gradients equatorward (see schematic in Figure 1a). During the summer months, the tropical boundaries move poleward. The surf zone breaks down at the end of the winter. Mixing is less strong in the summertime hemisphere than in the wintertime hemisphere as the easterly winds do not support planetary-scale wave breaking, and the region of sharp tracer gradients moves poleward. While each tracer-based width exhibits this broad pattern, their seasonal cycles are distinct and influenced by the amount of chemical loss taking place at each pressure level.

4.2. Tracer-Based Widths Near the Tropical Tropopause

We expect a relationship between the width of the tropics determined by tracer concentrations in the lower stratosphere above the tropical tropopause and tropical width as derived from tropopause height-based metrics. To understand this relationship, we correlate the three tropopause height based metrics in Table 1 with the tracer-based metrics at 73 mb. We conduct these correlations in a manner that takes

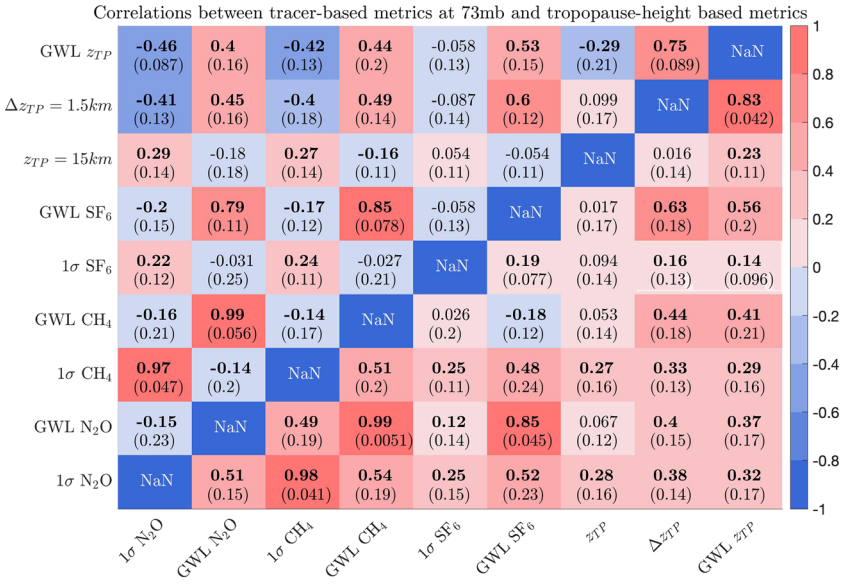

Figure 8. Correlations between deseasonalized tracer-based at 73mb (just above the tropical tropopause) and deseasonalized tropopause height-based metrics, with the Pearson's correlation coefficient printed (and bolded if correlations are significant at 95% level). The correlations are conducted on widths measured from each ensemble that are joined together into one data series. The upper triangle (above the diagonal line marked by NaN correlations) is the Northern Hemisphere and the lower triangle (below the diagonal line marked by NaN correlations) is the Southern Hemisphere. In brackets below the correlation coefficient is the standard deviation of correlations from each ensemble member.

advantage of the dynamical variability represented by the 10 ensemble members. Annual means of widths (1995–2024) measured from each ensemble member are calculated and are appended to each other to form one long data series with 300 datapoints, containing widths from all 10 ensemble members. Correlations are conducted and presented in Figure 8. Also presented in brackets is the standard deviation of correlations measured in each individual ensemble member.

The contours of N_2O and CH_4 and of N_2O and SF_6 track each other closely in the lower stratosphere as shown in Figures 1b and 1c. We therefore expect widths derived from tracer concentrations to correlate. Strong correlations exist between tracer-based widths measured from the same metric in both hemispheres in Figure 8. At 73mb, correlations are stronger in the Southern Hemisphere than in the Northern Hemisphere when widths from different tracer-based metrics are correlated. Correlations between widths from the conserved tracer SF_6 and tracers experiencing chemical loss (N_2O and CH_4) are as high as correlations between N_2O and CH_4, with similar standard deviation between ensemble members. (In section 4.4, we correlate tracer-based widths in the upper and middle stratosphere.)

Tropopause height-based metrics correlate well with each other, particularly the two tropopause break metrics ($\Delta z_{TP} = 1.5$ km and GWL in tropopause height). Correlations shown in Figure 8 fall into the range given in Table 4 of Davis and Rosenlof (2012) (which they presented for the Northern Hemisphere only) except for the $z_{TP} = 15$ km in the Northern Hemisphere. Figure S11 shows that the $z_{TP} = 15$ km metric does not vary in the same way as the $\Delta z_{TP} = 1.5$ km and GWL in tropopause height do in the Northern Hemisphere. Therefore, its correlation with the two tropopause break metrics is weak.

The tropopause break metrics ($\Delta z_{TP} = 1.5$ km and GWL of tropopause height) correlate well with tracer-based metrics in both hemispheres. In the Northern Hemisphere, correlations between GWL tracer widths and tropopause break widths are positive while correlations between 1σ widths and the two tropopause break widths are negative. In the Southern Hemisphere, GWL tracer width and tropopause break width correlations are generally strongly positive and correlations between tropopause break widths and 1σ widths are weakly positive. In both hemispheres, the $z_{TP} = 15$ km correlates more weakly with tracer based widths than GWL of z_{TP} and $\Delta z_{TP} = 1.5$ km (Figure S11). Finally, we note that GWL of z_{TP} is an

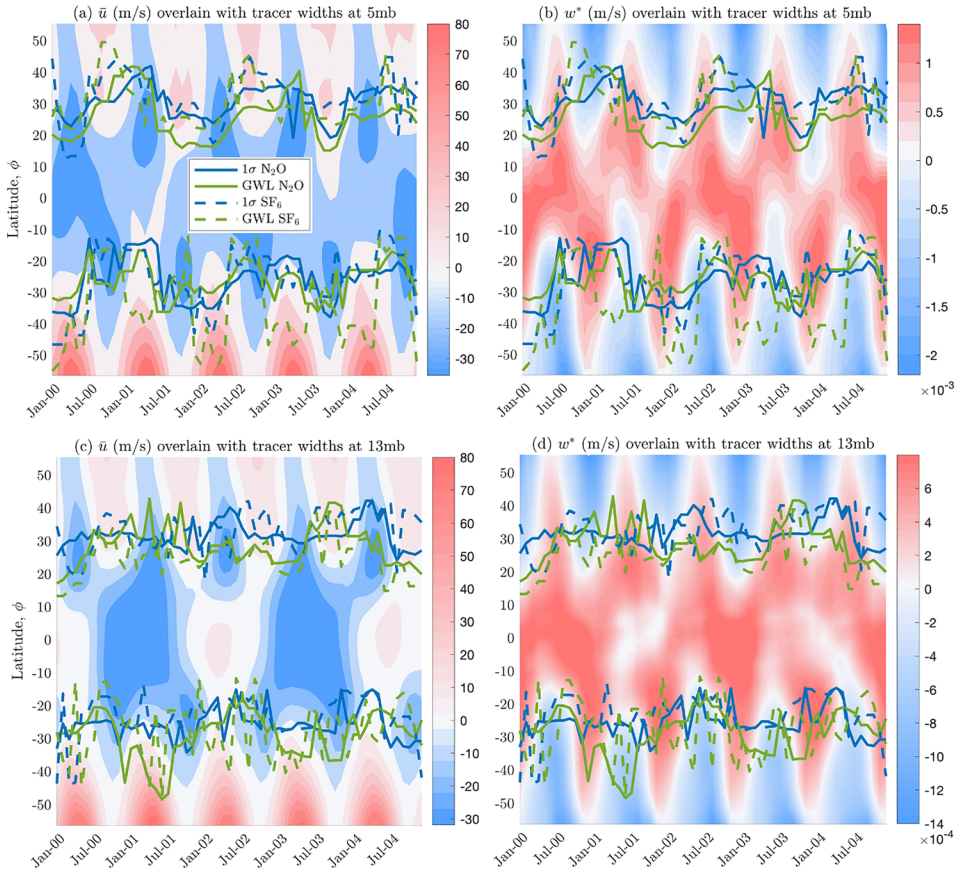

Figure 9. Tracer widths measured from ensemble mean monthly output underlain by (left column) zonal mean zonal wind and (right column) w^* at the following vertical levels: (first row) 5mb and (second row) 13mb. Blue represents regions of easterlies (left) and downwelling (right), and red represents westerlies (left) and upwelling (right) regions. The tracer widths have been lagged by τ_χ. The 1σ widths are plotted in blue and the GWL widths are plotted in green.

objective metric that does not depend on a prescribed threshold, unlike $z_{TP} = 15$ km and $\Delta z_{TP} = 1.5$ km (Davis & Rosenlof, 2012). The correlations between tracer-based widths and this objective metric GWL z_{TP} are generally strong in both hemispheres.

In summary, the GWL widths correlate strongly with each other, the 1σ widths correlate strongly with each other, and the GWL widths correlate with tropopause-height based widths in both hemispheres. Therefore, tropical width in the lower stratosphere as measured by tracer-based GWL widths are related to the latitude of the break in tropopause height. This suggests a key conclusion: that the widths in the lower stratosphere and at the tropopause are linked.

4.3. Comparing Middle and Upper Stratospheric Tracer Widths to Dynamical Metrics $\overline{u} = 0$ and $w^* = 0$

The seasonal cycle in tracer widths is influenced by patterns of zonal wind and residual vertical velocity. We overlay tracer widths on zonal wind (Figures 9a and 9c) and residual vertical velocity (Figures 9b and 9d) at 5mb and 13mb over the five-year period 2000–2004 and discuss first this qualitative comparison. We then correlate these widths over 30 years of simulation.

Both the residual circulation and mixing contribute to the equatorward shift of the widths during the winter and to the poleward shift of widths in the summer. The intrusion of westerlies causes planetary-scale wave breaking in the wintertime surf zone (Figures 9a and 9c). These processes steepen tracer gradients (Figure 7) due to enhanced mixing induced by wave breaking. This contributes to a contraction of the tropics (i.e., an equatorward shift) in the winter hemisphere. During the winter, the region where upwelling motion switches to downwelling motion is more equatorward than during the summer (Figures 9b and 9d).

Vertical ascent induces steeper tracer gradients towards the equator (Holton, 1986). In the winter, the strong meridional tracer gradient follows the equatorward shift of differential vertical advection at the turnaround latitude.

Summer easterlies cannot support Rossby wave propagation, which shuts down Rossby wave mixing and weakens residual circulation transport. In regions where chemical loss is significant, we expect photochemistry, which typically has a smoother latitudinal profile than mixing or vertical velocity, to become a dominant influence on tracer concentration profiles. Consequently, the region of steeper gradient is farther poleward. At the start of the summer when the surf zone breaks down, the widths move slightly poleward (as the region of ascent expands poleward). The widths then move equatorward as the wintertime surf zone forms again. Therefore, both large-scale vertical motions and mixing drive the 1σ and GWL widths to be further poleward in the summer months than in the winter.

We note examples of brief disruptions to the velocity fields and their comparison to the lagged tracer fields in Figure 7. For example, in July–December 2003 in the Northern Hemisphere, the $\overline{u} = 0$ region extends equatorward over a deep latitudinal extent. Disruptions also occur in the vertical velocity field: for example, November 2000–May 2001 at 13mb, the region of upwelling is disrupted by a layer of air that is not experiencing vertical motion (i.e., $w^* \approx 0$ in Figure 9d). This layer of air extends from the equatorial region towards the Northern Hemisphere tropics. The N_2O and CH_4 widths follow the $w^* = 0$ line formed between this stationary airmass and upwelling air. This disruption in the ascent of air allows N_2O and CH_4 to undergo chemical destruction at equatorial latitudes, breaking up the region of high N_2O and CH_4 concentrations near the Equator (Figures 7c and S10b). These disruptions affect 1σ width measurements of long-lived tracers N_2O and CH_4, thus demonstrating the value of measuring widths from different tracers and by different metrics.

Finally, we note that in these examples the GWL CH_4, N_2O, and SF_6 widths occasionally mark the sharp tracer contours that form as a result of the easterly winds and/or the region of ascent extending poleward (e.g., SF_6 GWL widths in the southern hemisphere in January of 2002–2004 in Figure 9b). In contrast, the 1σ widths measured on all three tracers consistently identify steep features in *tropical* tracer contours. This is another reason why measuring widths from different metrics and tracers is valuable.

We next compare tracer-based widths and two dynamical measures of tropical width: the $\overline{u} = 0$ metric, which measures the critical level at which mixing becomes important, and the $w^* = 0$ metric, which measures the turnaround latitude between ascending and descending motion. Colocated metrics do not necessarily indicate the same variability nor responses to forcings (Waugh et al., 2018). We therefore correlate these dynamical metrics with tracer metrics over the 30-year period 1995–2024 during December–February in the Northern Hemisphere (5mb and 13mb) and in the Southern Hemisphere during March–May (5mb) and July–September (13mb) and present the correlations in Figure 10. These are months when the tracer widths fall over the $\overline{u} = 0$ and $w^* = 0$ lines in Figure 9. As in section 4.2, prior to conducting the correlations, we stitch together each ensemble member time series for each set of widths measured. We perform cross correlations on these data series, indicate in bold font the correlations that are significant at the 95% level, and note in parentheses the standard deviation of the correlations conducted on individual ensemble members (Figures 10 and S12).

We first discuss correlations between dynamical and tracer-based metrics during the winter months (Figure 10). We find some positive correlations in the Northern Hemisphere during December–February at 5mb and 13mb between the $\overline{u} = 0$ metric or the $w^* = 0$ metric and the lagged tracer-based metrics (Figure 10). For example, in Figure 10a, the correlation between $\overline{u} = 0$ and $w^* = 0$ is weakly positive in the both hemispheres. During March–May, in the Southern Hemisphere, the $\overline{u} = 0$ and $w^* = 0$ metrics correlate more strongly with several tracer-based widths than during December–February in the Northern Hemisphere. In contrast at 13mb in the Northern Hemisphere during December and January (Figure 10b), the $w^* = 0$ and the $\overline{u} = 0$ metrics correlate weakly and there are weak correlations between the dynamical and tracer-based metrics. We note that gravity wave propagation and breaking occur at these altitudes, which do not follow the stationary Rossby wave heuristic of $\overline{u} = 0$ as the critical latitude. Gravity waves drive a substantial fraction of the residual circulation, which explains the weak correlations between both $\overline{u} = 0$ and $w^* = 0$, and between dynamical and tracer-based metrics at this altitude.

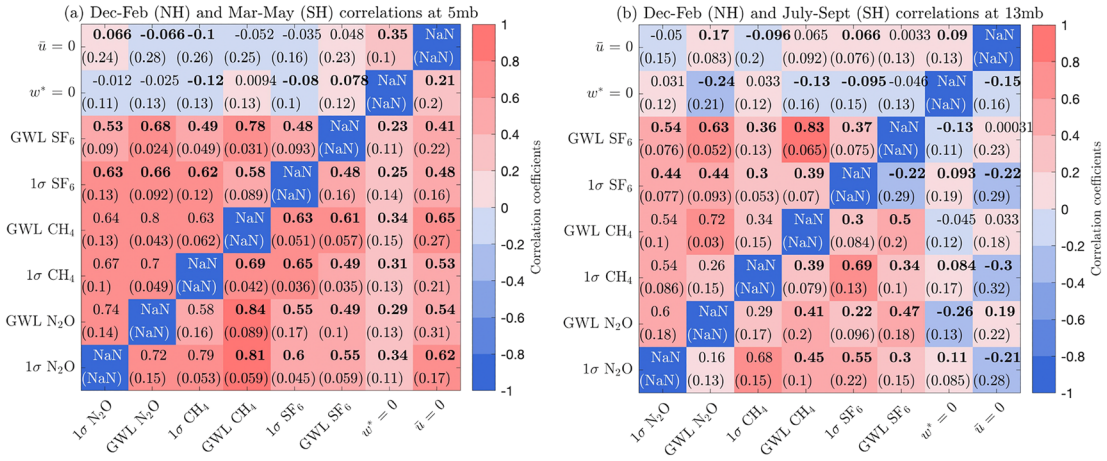

Figure 10. Correlations 1995–2024 between the mean tracer and dynamical widths measured from each ensemble that are joined together into one time-series at (a) 5mb and (b) 13mb. The tracer widths have been lagged by τ_χ. Each panel shows Pearson correlation coefficients, with the upper triangle correlating Northern Hemisphere and the lower triangle showing Southern Hemisphere correlations. Bolded correlations are significant at 95% level. In brackets is the standard deviation of correlations from each ensemble member.

We now discuss months where the lagged tracer-based widths do not follow the $w^* = 0$ and the $\overline{u} = 0$ lines in Figure 9. Figure S12 presents correlations at the same pressure levels as Figure 10 for the months leading up to the summer: April-–June in the Northern Hemisphere and October–December in the Southern Hemisphere. During these months, the tracer-based widths shift in the opposite meridional direction to dynamics-based widths: for example, in the southern hemisphere during November and December, the tracer-based widths are more equatorward than the $w^* = 0$ and the $\overline{u} = 0$ lines which extend poleward (Figure 9). Therefore, most correlations between tracer-based widths and dynamical widths are weak in Figure S12.

Finally, we note that correlations amongst tracer-based widths are generally strong and significant between N_2O, CH_4, and SF_6 metrics in Figure 10. Correlations between long-lived tracers N_2O and CH_4 in the Northern Hemisphere are not significant but are generally as high as other tracer-tracer correlations (Figure 10). Widths measured from different tracers and using different tracer metrics correlate well when their chemical lifetimes are similar and when zonal winds and vertical velocities influence each tracer's contours similarly (Figures 7, 9, and 10). During months when widths from different metrics behave differently in the midstratosphere (Figures 9c and 9d), correlations between tracer-based widths are strong only when widths measured by the same metric are correlated (Figure S12b).

5. Conclusions

Existing tropical width studies focus on the troposphere using metrics that are predominantly based on derived dynamical quantities, such as the stream function and tropopause height. Consistently measuring stratospheric tropical width increases the toolkit for probing stratospheric dynamical and transport processes. Further, some proposed mechanisms for tropospheric tropical expansion include stratospheric influences. This study's development of tracer metrics for stratospheric tropical width and its treatment of physical influences on tracer-based tropical width helps to lay the foundation for future work to assess trends in stratospheric tropical width as well as feedbacks between the stratosphere and the troposphere that could influence tropical width.

Understanding stratospheric width-determining mechanisms can be expected to benefit from an understanding of the tropical widths that characterize long-lived, active tracers and their comparison to dynamical variables. Dynamical metrics explored in this study measure influences of large-scale stratospheric motions on tropical width, namely, the overturning circulation, the start of the westerlies in winter and horizontal mixing. We examined three tracers in this study: CH_4, N_2O, and SF_6. Their contours are influenced by vertical and horizontal advection and mixing, while long-lived tracers CH_4 and N_2O are also influenced by

chemical loss. Tracer metrics are sensitive to how these dynamical processes interact with each other and with chemical loss processes during transport. Two new metrics for using tracer concentrations to measure tropical width have been identified in this research: the 1σ method and the GWL method.

We analyzed the robustness of tracer metrics to spatial and temporal resolution using CESM1 WACCM4 model output. The 1σ and GWL methods applied to 3-D spatial data produce results that are more consistent between CH_4 and N_2O than the PDF method previously presented in other studies. In order to calculate a monthly tropical width, the PDF method requires 3-D tracer data at daily resolution. In contrast, the 1σ and GWL methods can be used on data at both daily and monthly timescales and can be applied throughout the depth of the stratosphere from 1mb to 100mb (i.e., over a deeper vertical extent than the previously proposed PDF method which is applicable above 30mb only). Further, they are consistently applicable at all times of year. Differences between widths measured from 2-D and 3-D data for the 1σ and GWL methods are low ($\pm 0.4^{o}$). Differences between 1σ widths measured on 2-D and 3-D data have a larger standard deviation across the 10 ensemble members than GWL widths. Widths from 2-D and 3-D data for the 1σ and GWL methods are very highly correlated throughout the stratosphere, suggesting that both the 1σ and GWL metrics can be applied to 2-D data for some applications.

We examined key physical processes measured by tracer-based widths. Tracer contours can be expected to be influenced by horizontal and vertical motions on a delay timescale, which is the ratio of the *e*-folding scale height to the residual vertical velocity. Tracer widths lagged by this delay timescale exhibit a seasonal cycle where tropical boundaries move equatorward during winter months, because of the strong mixing in the surf zone that steepens gradients at its equatorward edge. Tropical boundaries marked by tracer widths move poleward during summer months because tropical tracer contours in the summertime are less steep than in the wintertime, due to the lack of mixing. Lagged tracer widths were then correlated with dynamical widths, specifically with the turnaround latitude $w^* = 0$ and the critical level $\overline{u} = 0$. During the early winter months, tracer-based widths correlate well with dynamical widths. They are less well correlated with the $\overline{u} = 0$ and $w^* = 0$ metrics during the months preceding summer months. In the lower stratosphere above the tropical tropopause, the tracer-based widths correlate well with widths derived from tropopause height, indicating a relationship between upper tropospheric and lower stratospheric width metrics. Tracer-based widths correlate strongly with each other at pressure levels where the tracers' chemical lifetimes are similar. Finally, at lower stratospheric pressure levels where mixing is stronger than in the upper stratosphere, tracer widths measured from the same metric but from different tracers correlate more strongly than tracer widths measured from different metrics and from different tracers.

The 1σ and GWL tropical width metrics are statistically robust and successful at determining the relationships and seasonal variability between stratospheric tracers and the circulation. These results advance opportunities to calculate trends in stratospheric tropical width under the influence of ozone depletion and anthropogenic greenhouse gas emissions, to probe mechanisms that set annual and long-term variability of stratospheric tropical width and to analyze relationships between and discover mechanisms for influences between tropospheric and stratospheric width.

Data Availability Statement

Model results shown in this paper are available online (https://acomstaff.acom.ucar.edu/dkin/JGR_Shah_2020/). The scripts that calculate tropical widths from the 1σ and GWL metrics are available at the repository link (https://doi.org/10.6084/m9.figshare.c.5086295.v1).

Acknowledgments

K. S. and S. S. were supported by grants from the National Science Foundation (NSF) 1539972 and 1848863. D. W. J. T. is supported by NSF AGS-1848785. This research was enabled by the computational and storage resources of NCAR's Computational and Information Systems Laboratory (CISL), sponsored by the NSF. D. E. K. was partly supported by NSF FESD-1338814. Cheyenne: HPE/SGI ICE XA System (NCAR Community Computing). Boulder, CO: National Center for Atmospheric Research (doi:10.5065/D6RX99HX).

References

Abalos, M., Polvani, L., Calvo, N., Kinnison, D., Ploeger, F., Randel, W. J., & Solomon, S. (2019). New insights on the Impact of Ozone-Depleting Substances on the Brewer-Dobson Circulation. *Journal of Geophysical Research: Atmospheres*, *124*, 2435–2451. https://doi.org/10.1029/2018JD029301

Brasseur, G. P., & Solomon, S. (2005). *Aeronomy of the middle atmosphere: Chemistry and physics of the stratosphere and mesosphere* (Vol. 3). Dordrecht, The Netherlands: Springer science & business media.

Charlton-Perez, A. J., Baldwin, M. P., Birner, T., Black, R. X., Butler, A. H., Calvo, N., et al. (2013). On the lack of stratospheric dynamical variability in low-top versions of the CMIP5 models. *Journal of Geophysical Research: Atmospheres*, *118*, 2494–2505. https://doi.org/10.1002/jgrd.50125

Davis, S. M., Hassler, B., & Rosenlof, K. H. (2018). Revisiting ozone measurements as an indicator of tropical width. *Progress in Earth and Planetary Science*, *5*, 1–11. https://doi.org/10.1186/s40645-018-0214-5

Davis, S. M., & Rosenlof, K. H. (2012). A multidiagnostic Intercomparison of tropical-width time series using reanalyses and satellite observations. *Journal of Climate*, *25*(4), 1061–1078. https://doi.org/10.1175/JCLI-D-11-00127.1

Grise, K. M., Davis, S. M., Simpson, I. R., Waugh, D. W., Fu, Q., Allen, R. J., et al. (2019). Recent tropical expansion: Natural variability or forced response? *Journal of Climate*, *32*, 1551–1571. https://doi.org/10.1175/JCLI-D-18-0444.1

Holton, J. R. (1986). A dynamically based transport parameterization for one-dimensional photochemical models of the stratosphere. *Journal of Geophysical Research*, *91*(D2), 2681–2686. https://doi.org/10.1029/JD091iD02p02681

Hudson, R. D., Andrade, M. F., Follette, M. B., & Frolov, A. D. (2006). The Total Ozone Field Separated Into Meteorological Regimes. Part II: Northern Hemisphere mid-latitude total ozone trends.

Hudson, R. D., Frolov, A. D., Andrade, M. F., & Follette, M. B. (2003). The total ozone field separated into meteorological regimes. Part I: Defining the regimes. *Journal of the Atmospheric Sciences*, *60*(14), 1669–1677. https://doi.org/10.1175/1520-0469(2003)060<1669:TTOFSI>2.0.CO;2

Lamarque, J.-F., & Solomon, S. (2010). Impact of changes in climate and halocarbons on recent lower stratosphere ozone and temperature trends. *Journal of Climate*, *23*(10), 2599–2611. https://doi.org/10.1175/2010JCLI3179.1

Leovy, C. B. (1987). *Middle atmospheric dynamics*. Orlando, Florida: Academic Press.

Lucas, C., Timbal, B., & Nguyen, H. (2014). The expanding tropics: A critical assessment of the observational and modeling studies. *WIREs Climate Change*, *5*(1), 89–112. https://doi.org/10.1002/wcc.251

Neu, J. L., Sparling, L. C., & Plumb, R. A. (2003). Variability of the subtropical "edges" in the stratosphere. *Journal of Geophysical Research*, AC 10–1-17, *108*(D15), 4482. https://doi.org/10.1029/2002JD002706

Plumb, R. A. (1996). A "tropical pipe" model of stratospheric transport. *Journal of Geophysical Research*, *101*(D2), 3957–3972. https://doi.org/10.1029/95JD03002

Seidel, D. J., Fu, Q., Randel, W. J., & Reichler, T. J. (2008). Widening of the tropical belt in a changing climate. *Nature Geoscience*, *1*(1), 21–24. https://doi.org/10.1038/ngeo.2007.38

Solomon, A., Polvani, L. M., Waugh, D. W., & Davis, S. M. (2016). Contrasting upper and lower atmospheric metrics of tropical expansion in the southern hemisphere. *Geophysical Research Letters*, *43*, 10,496–10,503. https://doi.org/10.1002/2016GL070917

Sparling, L. C. (2000). Statistical perspectives on stratospheric transport. *Reviews of Geophysics*, *38*(3), 417–436. https://doi.org/10.1029/1999RG000070

Staten, P. W., Grise, K. M., Davis, S. M., & Birner, T. (2018). Re-examining tropical expansion. *Nature Climate Change*, *8*, 768–775. https://doi.org/10.1038/s41558-018-0246-2

Stiller, G. P., Fierli, F., Cagnazzo, C., Funke, B., Haenel, F. J., Reddmann, T., et al. (2017). Shift of subtropical transport barriers explains observed hemispheric asymmetry of decadal trends of age of air. *Atmospheric Chemistry and Physics*, *17*, 11,177–11,192. https://doi.org/10.5194/acp-17-11177-2017

Waugh, D., Grise, K. M., Seviour, W. J., Davis, S. M., Davis, N., Adam, O., et al. (2018). Revisiting the relationship among metrics of tropical expansion. *Journal of Climate*, *31*, 7565–7581. https://doi.org/10.1175/JCLI-D-18-0108.1